Organic Electronics 13 (2012) 1068–1072

Contents lists available at SciVerse ScienceDirect

Organic Electronics

journal homepage: www.elsevier.com/locate/orgel

Enhancement of the power conversion efficiency for organic photovoltaic devices due to an embedded rugged nanostructural layer

Dae Hun Kim [a], Young Pyo Jeon [a], Se Han Lee [a], Dea Uk Lee [a], Tae Whan Kim [a,*], Sung Hwan Han [b]

[a] Department of Electronics and Computer Engineering, Hanyang University, Seoul 133-791, Republic of Korea
[b] Department of Chemistry, Hanyang University, Seoul 133-791, Republic of Korea

ARTICLE INFO

Article history:
Received 6 December 2011
Received in revised form 24 February 2012
Accepted 26 February 2012
Available online 13 March 2012

Keywords:
Organic photovoltaic cells
Rugged structures
Power conversion efficiency

ABSTRACT

Organic photovoltaic (OPV) cells utilizing a rugged nanostructural layer were fabricated by using a mixed solution method. The charge separation at the heterointerface between the poly(3-hexylthiophene) (P3HT) nanostructural layer with a rugged surface and the C60 layer was increased due to an increase in the interfacial region between the donor and the acceptor layers, resulting in an increase in the short-circuit current density and the power conversion efficiency (PCE) of the OPV cells with a P3HT nanostructural layer. The PCE of the OPV cells with a nanostructural rugged layer is 30% higher than that without a rugged layer.

Photovoltaic cells have emerged as excellent candidates due to their promise as replacements for traditional fossil fuels. Organic photovoltaic (OPV) cells have currently been receiving considerable attention due to their high-mechanical flexibility and light weight [1–3]. OPV cells with a bilayer heterojunction structure have achieved power conversion efficiencies (PCEs) up to 5% [4,5], which is still far from the efficiency required for practical mass applications. The prospect of potential applications of OPV cells has led to substantial research and development efforts to enhance the PCE of OPV cells. The typical efficiency of OPV cells has been significantly affected by various factors of the light absorption efficiency, exciton dissociation efficiency, charge transport efficiency, and charge collection efficiency. OPV cells containing a nanostructural layer have been suggested to enhance their PCEs resulting from an increase in the dissociation efficiency of the excitons [6–8]. The exciton dissociation efficiency has played an important role for enhancing the device efficiencies of the OPV cells due to a short diffusion length of the exciton in organic materials. The PCE enhancement mechanisms of the OPV cells containing a nanostructural layer are attributed to two dominant factors. One factor for the PCE enhancement is related to an increase in the interfacial region between donor and acceptor materials. The increase in the charge separation for the active layer is attributed to an increase in the interfacial region between the donors and the acceptors [9–11]. Another factor for the PCE enhancement is attributed to the variation of the chain orientation. The P3HT chains of the nanostructural layer contain a partially oriented face, resulting in an achievement of the mobility of charges and a change of the energy levels [8,9,12]. Some studies on the fabrication of the high efficient OPV cells containing a nanostructural layer have been performed by using an anodized aluminum oxide template and an etching process [12,13], and other studies concerning the device performance for OPV cells fabricated utilizing polymer nanoparticles have been clarified that the PCE of OPV cells with nanoparticles decreases due to the poor morphology of the active layer [14–16].

Even though some studies concerning effects on thermal or solvent-vapor treatment on the photovoltaic characteristics of the OPV cells with conducting polymer/C60

* Corresponding author. Tel.: +82 2 2220 0354; fax: +82 2 2292 4135.
E-mail address: twk@hanyang.ac.kr (T.W. Kim).

1566-1199/$ - see front matter © 2012 Elsevier B.V. All rights reserved.
http://dx.doi.org/10.1016/j.orgel.2012.02.022

interpenetrating heterojunction structure have been performed [17,18], their PCEs are relatively unstable and low. Therefore, systematic investigations on the photovoltaic properties of the OPV cells with an embedded rugged nanostructural layer are still necessary to enhance their stability and PCE.

This letter reports data for the enhancement of the PCE for OPV cells with an embedded rugged nanostructural layer. Absorbance and photoluminescence (PL) measurements were performed to investigate the positions of the absorbance and PL peaks and the optical properties of the P3HT layer containing a rugged nanostructural layer, and atomic force microscopy (AFM) measurements were carried out to investigate the surface properties of the P3HT with a nanostructural layer. Current density–voltage (*J*–*V*) measurements were performed to investigate the device performance of the OPV cells based on a P3HT layer containing a rugged nanostrutural layer.

The OPV cells used in this study were formed on indium-tin-oxide (ITO)-coated glass substrates, and the sheet resistance of the ITO thin film was approximately 10 Ω/sq. After the surface of the chemically-cleaned ITO-coated glass substrates had been treated with an ultraviolet–ozone cleaner, the substrates were introduced into a glove box with a high-purity N_2 atmosphere. The poly (3,4-ethylenedioxythiophene):poly(styrenesulfonate) (PEDOT:PSS) solution was spin-coated onto the ITO-coated glass substrates by spin coating at 4500 rpm for 41 s in the glove box. Then, 1-wt% P3HT solution was spin-coated onto the PEDOT:PSS layer at a spin rate of 2000 rpm for 60 s and was annealed at 145 °C for 15 min. The solution for forming the nanostructural film was prepared by using a mixed solution of 1 ml of 0.5-wt% P3HT and 0.1 ml of propylene glycol mono-methyl ether acetate (PGMEA). After the mixed solution had been sonicated for 15 min, the mixed solution was spin-coated onto the PEDOT:PSS layer at a spin rate of 4500 rpm for 36 s and was annealed at 145 °C for 15 min. After the annealing process of the nanostructural layer, the nanostructural P3HT layer was formed. After the formation of the P3HT planar layer and the P3HT nanostructural layer, a C60 layer with a thickness of 40 nm was thermally evaporated in a vacuum chamber at a system pressure of approximately 8.5×10^{-7} Torr. Subsequently, the Liq cathode buffer layer was deposited on the active layer by using thermal evaporation; then, an Al layer with a thickness of 100 nm was formed. The active area of the fabricated cell was 2 mm × 2 mm. Finally, the fabricated OPV cells were annealed for 20 min at 145 °C on a hot plate. Twenty different devices with a P3HT rugged nanostructural layer were fabricated to achieve the reliability of the device characteristics under the same condition. Schematic diagrams of the fabricated Al/Liq/C60/P3HT/PEDOT:PSS/ITO cells with planar and rugged nanostructural layers are shown in Fig. 1a and 1b, respectively.

The AFM measurements were performed by using an XE-100 atomic force microscope, and PL measurements were carried out by using an ISS PC1 system. The PL measurements were carried out using a 75 cm monochromator equipped with an RCA 31034 photomultiplier tube. The excitation sources were the 440 or 560 nm line of a

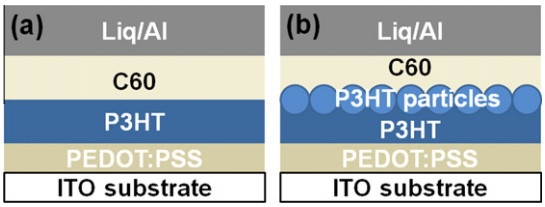

Fig. 1. Schematic diagrams of the organic photovoltaic cells utilizing (a) a planar film and (b) a P3HT nanostructural film.

He-Cd laser. The sample temperature was kept at 300 K. The *J*–*V* curves were measured in the dark and under an illumination by using a Keithley 2400 source meter. The photovoltaic characteristics were measured under AM 1.5 simulated illumination with an intensity of 100 mW/cm^2.

Fig. 2 shows absorbance and PL spectra for the P3HT molecular and the congregated P3HT particle in solution. The absorbance peaks for the dissolved P3HT molecular and the congregated P3HT particles appear at 440 and 560 nm, respectively. The PL peaks for the dissolved P3HT molecular and the congregated P3HT particles measured with an excitation wavelength of 440 nm appear around 575 and 660 nm, respectively. The red shifts of the absorbance and the PL spectra indicate that the fluorescence signal is dominantly attributed to intrachain aggregates, regardless of the small fraction of intrachain aggregates. The red shift of the interchain aggregates per particle plays the important role of energy acceptors for the large majority of chromophores [19]. The red shift of the interchain aggregates is attributed to efficient quenching of the conjugated polymer fluorescence due to variations in the numbers of quencher molecules [20–22] and polarons [23,24] and to intermittent fluorescence in the tightly-coiled conjugated polymer molecules [25–29].

Fig. 3 shows the PL spectrum for the mixed P3HT solution and its deconvoluted Gaussian functions measured with an excitation wavelength of 440 nm. The PL spectrum showed that the congregated P3HT particles were dissolved in a mixed solution. The peaks at 577 and 596 nm correspond to the P3HT molecular dissolved in the mixed

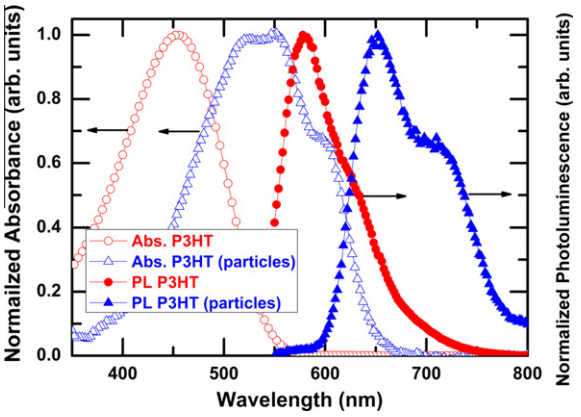

Fig. 2. Absorbance (empty) and PL (filled) spectra of the P3HT solution and the P3HT particle solution.

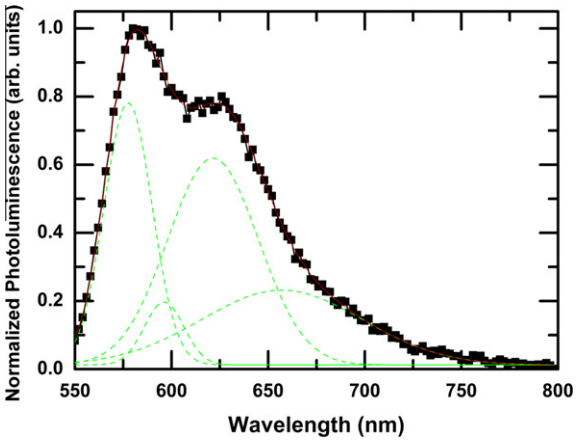

Fig. 3. PL spectrum of a mixture of the dissolved P3HT solution and the P3HT particle solution. The dashed lines represent the Gaussian functions of the PL spectrum.

solution, as shown in Fig. 2. The peaks at 621 and 657 nm correspond to the congregated P3HT particles in the mixed solution. It is noted that the two peaks from congregated P3HT particles in Fig. 3 are blue-shifted when compared with the peaks from congregated P3HT particles in Fig. 2 [19]. This blue shift is attributed to the fact that the congregated P3HT particles in the mixed solution of hydrophilic and hydrophobic solvents are smaller than those in the solution of only hydrophobic solvent. The existence of the congregated P3HT particle is confirmed by AFM images.

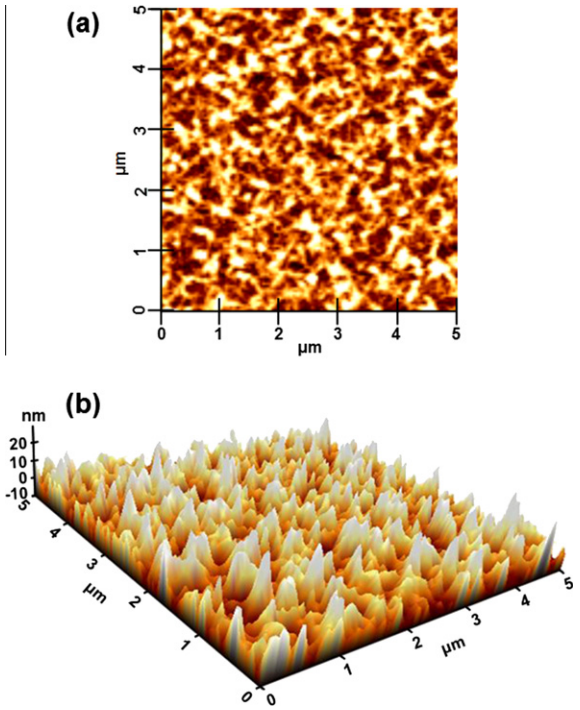

Fig. 4. (a) AFM and (b) AFM profile images of the nanostructural P3HT layer.

Fig. 4 shows the (a) AFM and the (b) AFM profile images of the nanostructural P3HT layer. The AFM image shows that the pore diameter of the fabricated nanostructural film with a rugged surface was between 100 and 200 nm. The AFM profile image shows that the thickness of the planar region for the nanostructural layer was about 10 nm. The thickness of the convex part of the nanostructural film was about 30 nm. The diameter and the height of the nanostructural layer depended significantly on the spin rate and the P3HT concentration of the mixed solution and on the ultrasonication treatment time. OPV cells with a nanostructural layer had a higher efficiency for exciton dissociation and for charge transport than those with a planar or a bulk heterojunction structural layer. Because the charge separation in OPV cells increases with increasing size of the interface between the donor and the acceptor layers, the transport of separated charges increases. Furthermore, the OPV cell with a nanostructural layer contains continuous paths, along which charges are easily moved, resulting in a decrease in charge recombination loss.

Fig. 5 shows (a) absorbance spectra of the P3HT and the P3HT nanostructural layers and (b) PL spectra for the

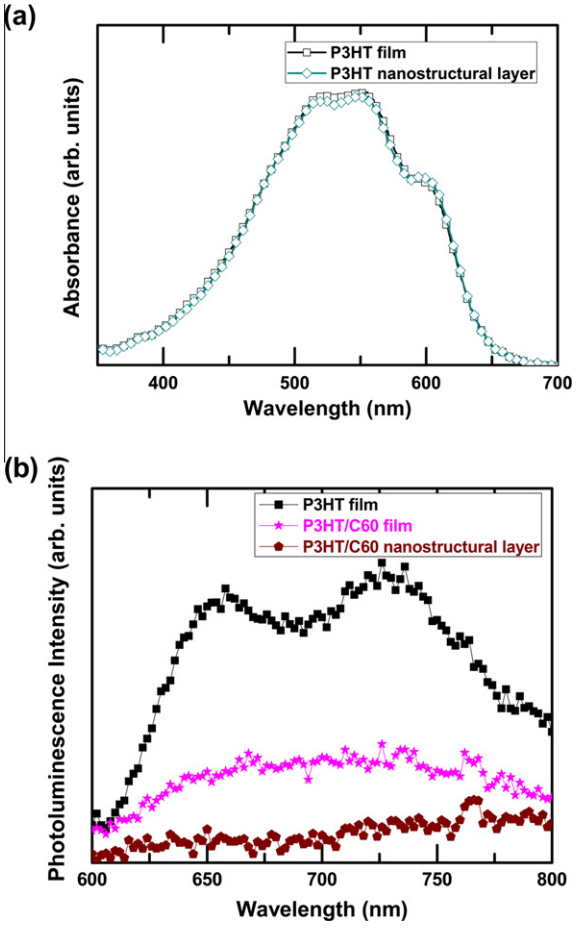

Fig. 5. (a) Absorbance spectra of the P3HT and the P3HT nanostructural layers and (b) PL spectra for the planar P3HT/C60 and the nanostructural P3HT/C60 layers.

planar P3HT/C60 and the nanostructural P3HT/C60 layers measured with an excitation wavelength of 560 nm. The absorbance spectrum of the P3HT nanostructural layer is similar to that of the P3HT layer. Because any additional peak for the absorbance spectrum of the P3HT nanostructural layer in comparison with that of the P3HT layer does not appear, the nanostructural layer has no impurities, undergoes no chemical transformations. The variation of the UV-absorbance spectrum has been explained on the basis of the variation of the P3HT chain orientation. The variation of P3HT chain orientation originates from the interfacial interaction between the P3HT and the PEDOT:PSS [12]. Because the UV-absorbance spectrum of the P3HT rugged nanostructure layer is similar to that of the P3HT planar layer, the chain orientation of the P3HT rugged nanostructure layer is analogous to that of P3HT planar layer. The change of the P3HT orientation might be not considered as an important mechanism factor for the PCE enhancement. The enhancement mechanism of the PCE for the OPV cells is dominantly attributed to an increase in the interfacial region between donor and acceptor materials. A quenching of the fluorescence intensity appears in the P3HT nanostructural layer, as shown in Fig. 5b. While the P3HT fluorescence of the planar layer is quenched by 59%, that of the nanostructural layer is quenched by 86%. This dramatic increase in quenching is attributed to efficient charge separation at the interface between the P3HT nanostructural layer and the C60. The increase in the interface region between the donor and the acceptor layers dramatically increases the separation of excitons, resulting in an increase in charge generation. Therefore, the magnitudes of the *Jsc* and the PCE are increased due to increased charge separation at the heterointerface between the P3HT nanostructural layer and the C60.

Fig. 6 shows the *J–V* results for OPV cells fabricated utilizing a P3HT nanostructural layer and a P3HT planar layer. The efficiencies of the OPV cells with planar P3HT/C60 layers and with nanostructural P3HT/C60 layers were 0.8% and 1.04%, respectively, and the corresponding *Jsc* values were 6.2 and 8.3 mA/cm^2. The error bars of the PCE values in the Fig. 6 indicate the maximum and minimum values of

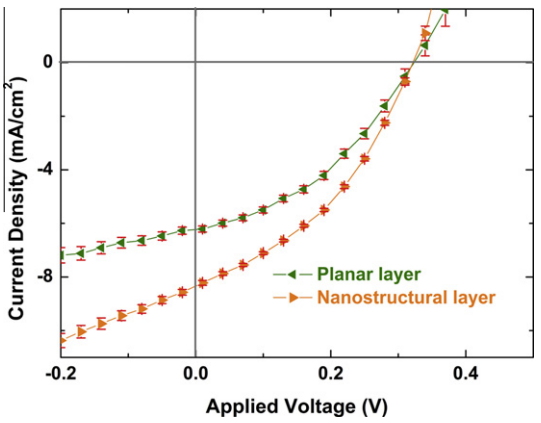

Fig. 6. Current density–voltage results of organic photovoltaic cells utilizing P3HT nanostructural and planar layers under 100 mW/cm^2.

Table 1
Device performances of organic photovoltaic cells utilizing a nanostructural P3HT layer and a planar P3HT layer.

P3HT/C60	*Jsc* (mA/cm^2)	*Voc* (V)	FF	η (%)
OPV cells with a planar layer	6.2	0.32	0.4	0.8
OPV cells with a nanostructural layer	8.3	0.32	0.39	1.04

20 different devices. The enhanced *Jsc* and PCE values can be attributed to the increased charge separation caused by the increased interface region between the donor and the acceptor layers. Device performances of OPV cells utilizing nanostructural P3HT and planar P3HT layers are summarized Table 1.

In summary, OPV cells utilizing a nanostructural layer with a rugged surface were fabricated utilizing a mixed P3HT solution. While the dissolved P3HT molecular formed a P3HT planar layer, the congregated P3HT particles generated a rugged surface layer on the P3HT planar layer. The interface region between the donor and the acceptor layers for the OPV cells with a nanostructural layer was larger than that for the OPV cells with a planar layer. The charge separation and the charge transport efficiencies were enhanced due to an increase in the interface region between the donor and the acceptor layers for OPV cells with a nanostructural layer. The PCE values of the OPV cells with planar P3HT/C60 and nanostructural P3HT/C60 layers were 0.8% and 1.04%, respectively, and the corresponding *Jsc* magnitudes were 6.2 and 8.3 mA/cm^2. The PCE and the *Jsc* values of the OPV cells were significantly improved by using a nanostructural layer with a rugged surface.

Acknowledgment

This research was supported by Basic Science Research Program through the National Research Foundation of Korea (NRF) funded by the Ministry of Education, Science and Technology (2011-0025491).

References

[1] C.J. Brabec, N.S. Sariciftci, J.C. Hummelen, Plastic solar cells, Adv. Funct. Mater. 11 (2001) 15–26.
[2] J.S. Kim, J.H. Park, J.H. Lee, J. Jo, D.Y. Kim, K. Cho, Control of the electrode work function and active layer morphology via surface modification of indium tin oxide for high efficiency organic photovoltaics, Appl. Phys. Lett. 91 (2007) 112111-1–112111-3.
[3] Y. Kim, S.A. Choulis, J. Nelson, D.D.C. Bradley, S. Cook, J.R. Durrant, Device annealing effect in organic solar cells with blends of regioregular poly(3-hexylthiophene) and soluble fullerene, Appl. Phys. Lett. 86 (2005) 063502-1–0363502-3.
[4] L.A.L. Ayzner, C.J. Tassone, S.H. Tolbert, B.J. Schwartz, Reappraising the need for bulk heterojunctions in polymer-fullerene photovoltaics: the role of carrier transport in all-solution-processed P3HT/PCBM bilayer solar cells, J. Phys. Chem. C 113 (2009) 50050–50060.
[5] K.H. Lee, P.E. Schwenn, A.R.G. Smith, G. Cavaye, P.E. Shaw, M. James, K.B. Krueger, I.R. Gentle, P. Meredith, P.L. Burn, Morphology of all-solution-processed "Bilayer" organic solar cells, Adv. Mater. 23 (2011) 766–770.
[6] J. Weickert, R.B. Dunbar, H.C. Hesse, W. Wiedemann, L. Schmidt-Mende, Nanostructured organic and hybrid solar cells, Adv. Mater. 23 (2011) 1810–1828.
[7] F. Yang, M. Shtein, S.R. Forrest, Controlled growth of a molecular bulk heterojunction photovoltaic cell, Nat. Mater. 4 (2005) 37–41.

[8] M. Aryal, K. Trivedi, W.W. Hu, Nano-confinement induced chain alignment in ordered P3HT nanostructures defined by nanoimprint lithography, ACS Nano. 3 (2009) 3085–3090.
[9] A.A. Bakulin, J.C. Hummelen, M.S. Pshenichnikov, P.H.M. van Loosdrecht, Ultrafast hole-transfer dynamics in polymer/PCBM bulk heterojunctions, Adv. Funct. Mater. 20 (2010) 1653–1660.
[10] R.A. Street, M. Schoendorf, Interface state recombination in organic solar cells, Phys. Rev. B 81 (2010) 205307-1–205307-12.
[11] L.H. Nguyen, H. Hoppe, T. Erb, S. Günes, G. Gobsch, N.S. Sariciftci, Effects of annealing on the nanomorphology and performance of poly(alkylthiophene):fullerene bulk-heterojunction solar cells, Adv. Funct. Mater. 17 (2007) 1071–1078.
[12] J.S. Kim, Y. Park, D.Y. Lee, J.H. Lee, J.H. Park, J.K. Kim, K. Cho, Poly(3-hexylthiophene) nanorods with aligned chain orientation for organic photovoltaics, Adv. Funct. Mater. 20 (2010) 540–545.
[13] F.A. Castro, H. Benmansour, C.F.O. Graeff, F. Nüesch, E. Tutis, R. Hany, Nanostructured organic layers via polymer demixing for interface-enhanced photovoltaic cells, Chem. Mater. 18 (2006) 5504–5509.
[14] C. Wu, Y. Zheng, C. Szymanski, J. McNeill, Energy transfer in a nanoscale multichromophoric system: fluorescent dye-doped conjugated polymer nanoparticles, J. Phys. Chem. C 112 (2008) 1772–1781.
[15] C. Wu, B. Bull, C. Szymanski, K. Christensen, J. McNeill, Multicolor conjugated polymer dots for biological fluorescence imaging, ACS Nano 2 (2008) 2415–2423.
[16] D. Tuncel, H.V. Demir, Conjugated polymer nanoparticles, Nanoscale 2 (2010) 484–494.
[17] V. Kittichungchit, T. Shibata, H. Noda, H. Tanaka, A. Fujii, N. Oyabu, M. Abe, S. Morita, M. Ozaki, Efficiency enhancement in organic photovoltaic cell with interpenetrating conducting polymer/C_{60} heterojunction structure by substrate-heating treatment, Jpn. J. Appl. Phys. 47 (2008) 1094–1097.
[18] V. Kittichungchit, T. Hori, H. Moritou, H. Kubo, A. Fujii, M. Ozaki, Effect of solvent vapor treatment on photovoltaic properties of conducting polymer/C_{60} interpenetrating heterojunction structured organic solar cell, Thin Solid Films 518 (2009) 518–521.
[19] C. Szymanski, C. Wu, J. Hooper, M.A. Salazar, A. Perdomo, A. Dukes, J. McNeill, Single molecule nanoparticles of the conjugated polymer MEH-PPV, preparation and characterization by near-field scanning optical microscopy, J. Phys. Chem. B 109 (2005) 8543–8546.
[20] L. Chen, D.W. McBranch, H.L. Wang, R. Helgeson, F. Wudl, D.G. Whitten, Highly sensitive biological and chemical sensors based on reversible fluorescence quenching in a conjugated polymer, Proc. Natl. Acad. Sci. USA 96 (1998) 12287–12292.
[21] B.S. Gaylord, A.J. Heeger, G.C. Bazan, DNA detection using water-soluble conjugated polymers and peptide nucleic acid probes, Proc. Natl. Acad. Sci. USA 99 (2002) 10954–10957.
[22] C.H. Fan, S. Wang, J.W. Hong, G.C. Bazan, K.W. Plaxco, A.J. Heeger, Beyond superquenching: hyper-efficient energy transfer from conjugated polymers to gold nanoparticles, Proc. Nat. Acad. Sci. USA 100 (2003) 6297–6301.
[23] M. Deussen, M. Scheidler, H. Bassler, Electric field-induced photoluminescence quenching in thin-film light-emitting diodes based on poly(phenyl-p-phenylene vinylene), Synth. Met. 73 (1995) 123–129.
[24] J.D. McNeill, D.B. O'Connor, D.M. Adams, S.B. Kämmer, P.F. Barbara, Field-induced photoluminescence modulation of MEH-PPV under near-field optical excitation, J. Phys. Chem. B 105 (2001) 76–82.
[25] D.A. Vanden Bout, W.T. Yip, D.H. Hu, D.K. Fu, T.M. Swager, P.F. Barbara, Discrete intensity jumps and intramolecular electronic energy transfer in the spectroscopy of single conjugated polymer molecules, Science 277 (1997) 1074–1077.
[26] D. Hu, J. Yu, P.F. Barbara, Single-molecule spectroscopy of the conjugated polymer MEH-PPV, J. Am. Chem. Soc. 121 (1999) 6936–6937.
[27] D. Hu, J. Yu, K. Wong, B. Bagchi, P.J. Rossky, P.F. Barbara, Collapse of stiff conjugated polymers with chemical defects into ordered, cylindrical conformations, Nature 405 (2000) 1030–1033.
[28] T. Huser, M. Yan, L. Rothberg, Single chain spectroscopy of conformational dependence of conjugated polymer photophysics, Proc. Natl. Acad. Sci. USA 97 (2000) 11187–11191.
[29] F. Schindler, J.M. Lupton, J. Feldmann, U. Scherf, A universal picture of chromophores in π-conjugated polymers derived from single-molecule spectroscopy, Proc. Natl. Acad. Sci. USA 101 (2004) 14695–14700.